LETTERS

# Strong crystal size effect on deformation twinning

Qian Yu[1], Zhi-Wei Shan[1,2], Ju Li[3], Xiaoxu Huang[4], Lin Xiao[1], Jun Sun[1] & Evan Ma[1,5]

**Deformation twinning[1–6] in crystals is a highly coherent inelastic shearing process that controls the mechanical behaviour of many materials, but its origin and spatio-temporal features are shrouded in mystery. Using micro-compression and *in situ* nano-compression experiments, here we find that the stress required for deformation twinning increases drastically with decreasing sample size of a titanium alloy single crystal[7,8], until the sample size is reduced to one micrometre, below which the deformation twinning is entirely replaced by less correlated, ordinary dislocation plasticity. Accompanying the transition in deformation mechanism, the maximum flow stress of the submicrometre-sized pillars was observed to saturate at a value close to titanium's ideal strength[9,10]. We develop a 'stimulated slip' model to explain the strong size dependence of deformation twinning. The sample size in transition is relatively large and easily accessible in experiments, making our understanding of size dependence[11–17] relevant for applications.**

Explosive growth in the use of small-volume materials such as submicrometre-scale single crystals is driving the exploration of sample-size-dependent mechanical behaviour[15–17]. At room temperature, the two major mechanisms responsible for the plasticity of materials are ordinary dislocation plasticity (ODP) and deformation twinning. For polycrystalline materials, it has been well-established that regardless of the major deformation mechanism, the apparent strength and the grain size ($d_g$) follows a Hall–Petch-type behaviour: $\sigma = \sigma_0 + kd_g^{-\alpha}$, where $\sigma$ is the flow strength, $\sigma_0$ and $k$ are size-independent constants and $\alpha$ is an exponent typically between 0.5 and 1. The difference is that the Hall–Petch slope for deformation-twinning-mediated plasticity ($k_{DT}$) is much larger (up to ten times) than that for ODP ($k_{ODP}$)[18–20]. In recent years, size effects on the plasticity of surface-confined single crystals have drawn considerable attention[15–17]. It has been demonstrated that the sample dimension $d$ strongly influences the ODP-mediated deformation and hence the apparent strength[15–17], which also follows a power-law behaviour. However, it is yet unknown if deformation-twinning-mediated plasticity would be strongly sample-size-dependent. If so, and if $k_{DT} \gg k_{ODP}$, the power-law scaling for deformation-twinning-mediated plasticity must break down at a much larger sample size than that for ODP-mediated plasticity, because the ideal strength of the crystal[9] imposes an upper bound on the flow stress—see Supplementary Fig. 1.

We chose a single-crystal Ti alloy as our model system. Deformation twinning is known to play a key part in the deformation of hexagonal-close-packed metals[7,8] owing to the limited number of dislocation slip systems. For compression of bulk Ti and α-Ti alloys along the *c*-axis[8,21–24], deformation twinning is the geometrically favoured deformation mode and the reported[8,21–24] twinning systems are $\{11\bar{2}2\}\langle\bar{1}\bar{1}23\rangle$, $\{11\bar{2}4\}\langle\bar{2}\bar{2}43\rangle$ and $\{10\bar{1}1\}\langle\bar{1}012\rangle$. In conventional samples, the twin lamellae in Ti and its alloys have thicknesses ranging from 0.1 to 10 μm and lengths of the order of several micrometres[7,8,21–24]. It is then interesting to see what will happen when the sample dimensions are reduced to the same scale or even smaller.

We used a bulk square Ti–5 at.% Al single crystal as the starting material, from which all the samples in this study were cut. The experimental details are described in the Methods and in the Supplementary Information. Supplementary Fig. 2 shows the behaviour of the bulk single crystal under [0001] compression. Profuse deformation twinning is seen, in agreement with the literature[24]. In micro-compression tests of pillars with $d \geq 1.0$ μm, almost all the deformed samples showed obvious shearing traces on the surfaces. Examples are shown in Fig. 1a and b. A trace analysis of the $d = 1.0$ μm micro-pillar showed that the shearing occurred on the $\{11\bar{2}2\}$ plane, which is a common twinning plane in hexagonal-close-packed Ti and its alloys. Electron backscatter diffraction (EBSD) analysis of these deformed pillars provides evidence that deformation twinning indeed occurred during compression. Figure 1c and d compare the pole figures of the $d = 8.0$ μm pillar, before and after the deformation. We observed nearly perfect {0001} reflection in the micro-pillar before loading, but after deformation several new orientations that are far from the initial orientation appeared. We identify these new orientations as due to deformation twinning on two types of twinning systems, $\{11\bar{2}2\}\langle\bar{1}\bar{1}23\rangle$, and $\{10\bar{1}1\}\langle\bar{1}012\rangle$, as indicated in Fig. 1d. Similar EBSD results were obtained for the $d = 1.0$ μm sample as well. Rapid deformation twin growth is also corroborated by the obvious strain bursts in the stress–strain curves; see Fig. 2a. Transmission electron microscopy (TEM) micrographs of the deformed $d = 8$ μm pillar, taken from its vertical cross-section cut using focused ion beam (FIB) micromachining (Supplementary Fig. 3), are shown in Supplementary Figs 4 and 5: deformation twins are observed inside tangles of curved dislocations. The twins with small sizes—that is, twin embryos—exhibit convex lens shapes (Supplementary Fig. 5), in contrast to the straight profile of grown twin bands (Supplementary Fig. 2).

We noticed remarkable changes in deformation behaviour for $d = 0.7$ μm and 0.4 μm. As shown in Fig. 3a and b, in these submicrometre pillars plastic deformation is concentrated on the top part of the pillar, resulting in a 'mushroom' shape. The load-displacement curve of this sample is given in Fig. 2b. In Fig. 2b we observe continuous plastic flow without any major strain burst. This difference from Fig. 2a suggests a dramatic change in the deformation mode as compared with the larger, micrometre-sized pillars.

We also conducted compression tests *in situ* inside a TEM for a 0.25-μm-diameter cylindrical pillar, to reveal the entire dynamic deformation process in these submicrometre pillars (see movie in the Supplementary Information). The still images comparing the structure before and after testing are displayed in Fig. 3c and d. The corresponding load-displacement curve is in Fig. 2c. Here again, we observe the development of mushroom-like sample morphology

[1]Center for Advancing Materials Performance from the Nanoscale (CAMP-Nano), State Key Laboratory for Mechanical Behavior of Materials, Xi'an Jiaotong University, Xi'an, 710049, China. [2]Hysitron Incorporated, 10025 Valley View Road, Minneapolis, Minnesota 55344, USA. [3]Department of Materials Science and Engineering, University of Pennsylvania, Philadelphia, Pennsylvania 19104, USA. [4]Danish-Chinese Center for Nanometals, Materials Research Division, Risø National Laboratory for Sustainable Energy, Technical University of Denmark, DK-4000 Roskilde, Denmark. [5]Department of Materials Science and Engineering, The Johns Hopkins University, Baltimore, Maryland 21218, USA.

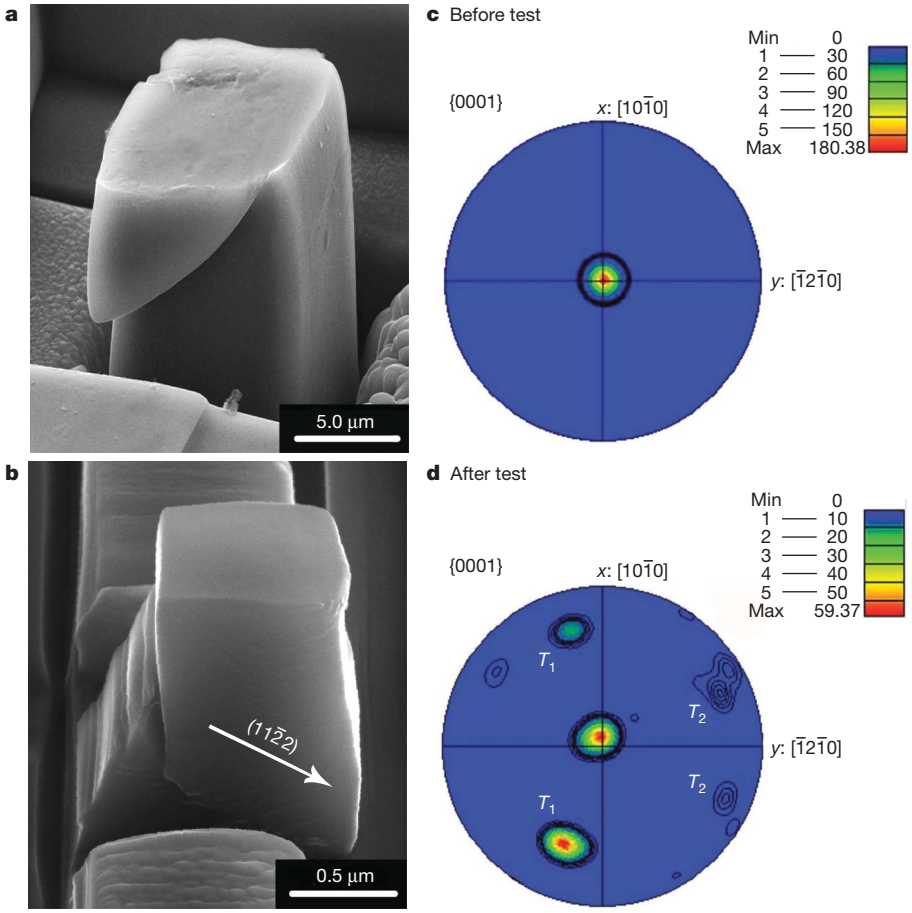


**Figure 1 | Scanning electron microscopy images of the deformed micropillars and EBSD pole figure.** **a**, $d = 8.0\,\mu m$. **b**, $d = 1.0\,\mu m$. **c**, **d**, EBSD pole figure of the $d = 8.0\,\mu m$ pillar before (**c**) and after (**d**) compression. $T_1$: $\{11\bar{2}2\}\langle\bar{1}\bar{1}23\rangle$ and $T_2$: $\{10\bar{1}1\}\langle\bar{1}012\rangle$denote the twin type. $T_1$ and $T_2$ have misorientation of $64^\circ/<1\bar{1}00>$ and $57^\circ/<2\bar{1}\bar{1}0>$, respectively, with respect to the initial orientation. (Half-width $10^\circ$; cluster size $5^\circ$.)

and continuous plastic flow. TEM micrographs in Fig. 3c show that before the test, the density of dislocations is very low, except at the top of the pillar where a few dislocation lines were left from FIB damage (our TEM examinations indicate that the damage layer is only a few nanometres thick and should not affect the mechanism transition at the size scale of $d_c \approx 1\,\mu m$). After the compression test, a high density of tangled dislocations is observed; see Fig. 3d. There is no sign of deformation twins from either the images or the diffraction patterns. The movie in the Supplementary Information, when correlated with Fig. 2c, reveals that during the first and second loading, only a few dislocations propagated from the contact surface into the pillar. The dislocation activities became intense only during the third loading, at which point the load reached $105\,\mu N$ (the corresponding contact stress is $\sim 2$ GPa, when dividing the load by the contact area). The continuous generation, multiplication and considerable accumulation of dislocations (see also Fig. 3d) are consistent with Fig. 2b and Fig. 2c: these submicrometre pillars exhibit smooth load-displacement curves in lieu of the large strain bursts corresponding to rapid deformation twin growth (Fig. 2a).

These results clearly demonstrate that deformation twinning is strongly dependent on the sample size. In micrometre-sized pillars, deformation twinning is still the dominant mode of plastic deformation, as in bulk-sized samples[8,21–24]. As shown in Fig. 2d for the pillars with $d \geq 1\,\mu m$, the strength (red symbols) and $d$ (here the strength values are defined as the true stress measured at the twinning events, that is, the bursts in Fig. 2a) clearly follow a Hall–Petch-type relationship with $\alpha \approx 1$. We note that this strong size effect on deformation twinning is intrinsic to the material, because sample tapering is absent and the very thin FIB damage layer on the surface should be negligible in these relatively large samples.

At submicrometre sample sizes, in contrast, deformation twinning is suppressed, giving way to ODP only, even though our loading direction is favourable for deformation twinning. In addition, strain bursts were not observed and the pillars were deformed into a mushroom-like geometry. For these submicrometre samples, we have defined the maximum flow stress as the peak load divided by the area of the narrowest cross-section $\pi d_{\mathrm{narrowest}}{}^2/4$ of the mushroomed pillars (see inset in Fig. 2d) and plotted it in Fig. 2d. It is interesting to find that the maximum flow stress saturated at close to the material's ideal strength[10], which is 2.8–4.9 GPa in pure shear for Ti[9].

We wondered why deformation twinning follows a power-law scaling on $d$, and why $k_{\mathrm{DT}} \gg k_{\mathrm{ODP}}$. Here we present a 'stimulated slip' model to explain the size dependence of deformation twinning. In contrast to ODP, where inelastic shear activities are randomly dispersed among slip planes, deformation twinning is characterized by perfectly correlated layer-by-layer shearing: all slip (twinning dislocations) on atomically adjacent parallel planes must have the same Burgers vector. We posit that deformation twinning in relation to ODP is akin to what laser (light amplification by stimulated emission of radiation)[25] is to normal light, in the sense of slip coherence.

Here we consider a cuboidal crystal with size $d$ and a total dislocation density $\rho$ (in units of $m^{-2}$). These stored lattice dislocations may penetrate a twinning slip plane $n$ of area $d^2$ (see Fig. 4). We assume that a small fraction $P_{\mathrm{promoter}}$ of the dislocations that penetrate plane $n$ can play the role of 'promoters' (for example screw dislocations in various pole mechanisms[2,6,26–28]), that 'stimulate' slip of the same character to occur also on the next atomic plane. Specifically, we assume that when a moving slip front (glide dislocation with twinning Burgers vector) on plane $n$ hits and wraps around a promoter, inelastic shear of the same character 'infects' plane $n+1$; and once infected anywhere on plane $n+1$, we assume this stimulated twinning slip will propagate and cover the entire plane $n+1$ as well, if the stress is high enough to drive it pass the forest dislocation obstacles, thickening the deformation twinning. The layer-to-layer 'infection probability' is simply

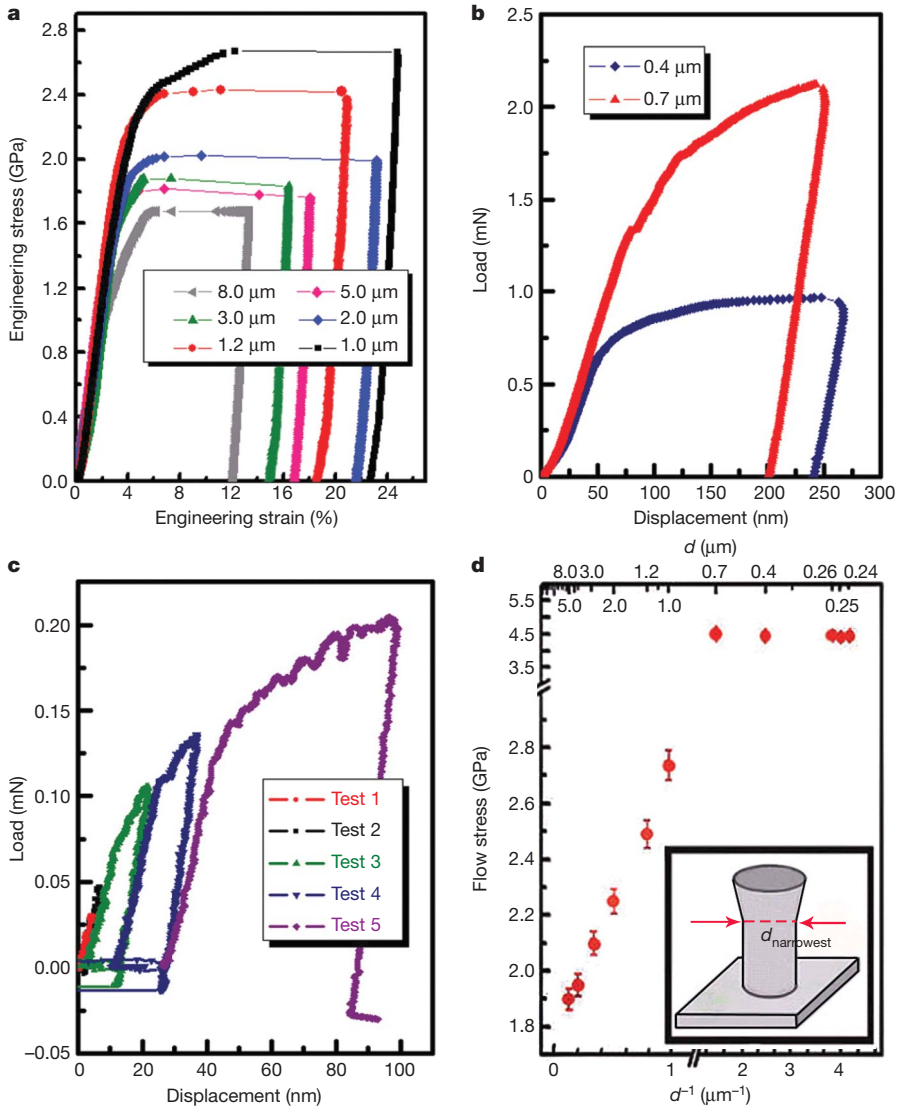


**Figure 2 | Mechanical data of the tested samples.** **a**, The stress–strain curves of micropillars with decreasing side length, $d$ from 8.0 to 1.0 μm. **b**, The load-displacement curves of submicrometre pillars. **c**, The load-displacement curves of a submicrometre cylindrical pillar with 0.25 μm diameter, in five consecutive load–unload steps during *in situ* testing inside a TEM (see movie in the Supplementary Information). The negative forces at the end of the unloading segments are due to adhesion between diamond tip and the pillars. **d**, Flow stress measured for the pillars versus $d$. We use the narrowest cross-section $\pi d_{\text{narrowest}}^2/4$ to calculate the flow stress. The error bars are two standard deviations.

$$P_{\text{infection}} \approx d^2 \rho P_{\text{promoter}} \quad (1)$$

Deformation twinning keeps thickening when

$$1 \approx P_{\text{infection}} \quad (2)$$

and the critical dislocation density necessary for the sudden transition to perfect slip coherence is thus

$$\rho_c \approx d^{-2} P_{\text{promoter}}{}^{-1} \quad (3)$$

From the Taylor hardening model[29]

$$\sigma = \sigma_0 + \kappa E b \rho^{1/2} \quad (4)$$

where $E$ is the Young's modulus, $b$ is the Burgers vector length, $\kappa$ is a dimensionless constant of order 1, $\sigma_0$ contains contributions from lattice friction, solute strengthening, and so on, we have the twinning stress

$$\sigma_{\text{DT}} = \sigma_0 + (\kappa E b P_{\text{promoter}}{}^{-1/2}) d^{-1} = \sigma_0 + k_{\text{DT}} d^{-1} \quad (5)$$

The best fit in Fig. 2d gives $\alpha = 0.976$, consistent with equation (5) above. The relatively large deformation twinning Hall–Petch slope $k_{\text{DT}}$ (see also Supplementary Table 1 and ref. 18) can be explained by a small $P_{\text{promoter}} \approx 10^{-2}$, which is reasonable because only a small subset of the stored dislocations may be screw poles of the right type for promoting twinning slip. A full discussion of this model is provided in the Supplementary Information.

A large $k_{\text{DT}}$ in $\sigma_{\text{DT}} = \sigma_0 + k_{\text{DT}} d^{-\alpha}$ drives early deformation-twinning abdication ($d_c \approx 1$ μm), because as $\sigma_{\text{DT}}$ approaches the ideal strength, there will be profuse dislocation nucleation, leading to high ODP strain rates. We note that as the pillars enter the submicrometre regime, the nucleation of ODP dislocations is increasingly assisted by the roughness left during FIB processing at the contact interface, and the now-very-large near-surface regions[30].

We conclude that deformation twinning is an intensely collective, 'stimulated slip' phenomenon, analogous to 'stimulated emission' in laser theory[25]. Stimulated slip from plane $n$ to plane $n+1$ is catalysed by promoter defects, such as screw dislocation poles[2,6,26–28]. Dual requirements must be met for deformation twinning: the stress needs to be high enough to drive a twinning dislocation to sweep plane $n$ of area $d^2$, cutting across forest obstacles; and of these forest obstacles, a sufficient proportion must be able to promote slip from plane $n$ to $n+1$. The smaller $d$ is, the more weakly two adjacent slip planes are effectively coupled by threading screw pole dislocations, and the more difficult it is for deformation twinning . The large Hall–Petch slope $k_{\text{DT}}$ implies a small promoter fraction $P_{\text{promoter}}$ among the stored bulk dislocations, leading to a very large $d_c$, observed to be ~1 μm, at which Hall–Petch behaviour breaks down and transition to incoherent ODP occurs.

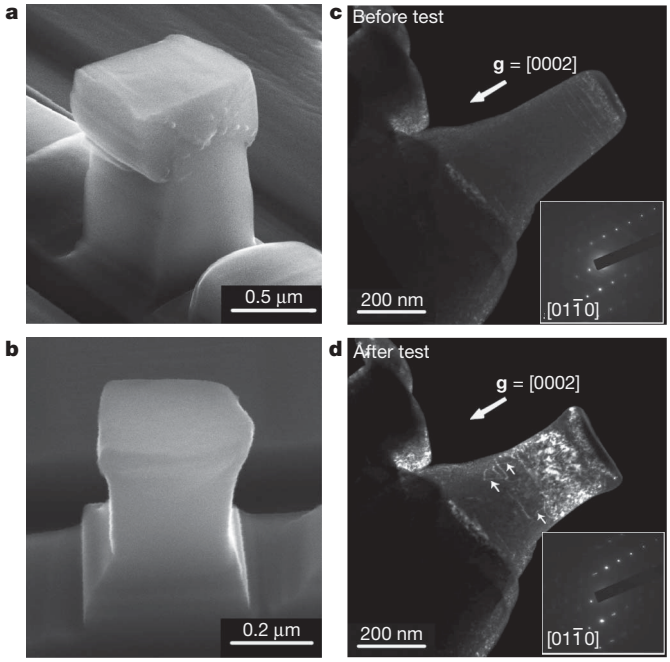


**Figure 3 | Electron microscopy images of the tested samples.** **a**, **b**, SEM images of the deformed $d = 0.7$ μm (**a**) and $d = 0.4$ μm (**b**) pillars. **c**, **d**, Centred dark-field TEM images with diffraction pattern (insets) of the 0.25-μm-diameter pillar before (**c**) and after (**d**) the *in situ* compression test. The beam direction was [01$\bar{1}$0] and the reflection vector **g** = [0002].

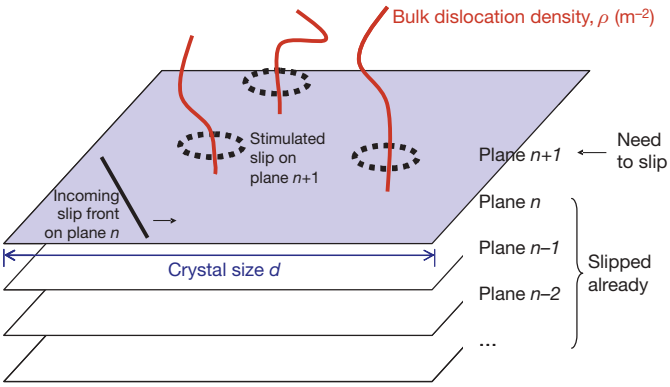


**Figure 4 | Schematic of the 'stimulated slip' model.** Thickening of deformation twin by 'stimulated slip' occurs when an incoming slip front (twinning glide dislocation) hits bulk screw dislocation 'promoters', a subset of the bulk forest dislocation population.

This size is of considerable technological importance. When the surface-bound contiguous crystal is reduced to the submicrometre scale, the effective interlayer coupling responsible for coherent 'stimulated slip' becomes so weak that deformation twinning is no longer triggered by bulk promoters, and incoherent ODP at high stress is sufficient to match the imposed strain rate. We note that the discussions above are based on a bulk promoter population, which scales with the volume. Deformation twinning proficiency may go up again at very small crystal sizes such as 10 nm (ref. 1), when the most effective promoters for stimulated slip may be grain boundaries and surfaces instead of screw dislocations, on the basis of an area-to-volume ratio argument.

## METHODS SUMMARY

The orientation of the single crystal α-Ti alloy was determined using the Laue back reflection method. The pillar samples oriented along the *c*-axis for compression testing were prepared using FIB. Compression testing was performed using an MTS Nanoindenter XP and a Hysitron TEM PicoIndenter, respectively.

**Received 13 July; accepted 17 November 2009.**

1. Chen, M. W. *et al.* Deformation twinning in nanocrystalline aluminum. *Science* **300,** 1275–1277 (2003).
2. Christian, J. W. & Mahajan, S. Deformation twinning. *Prog. Mater. Sci.* **39,** 1–157 (1995).
3. Ogata, S., Li, J. & Yip, S. Energy landscape of deformation twinning in bcc and fcc metals. *Phys. Rev. B* **71,** 224102 (2005).
4. Wu, X. L. & Zhu, Y. T. Inverse grain-size effect on twinning in nanocrystalline Ni. *Phys. Rev. Lett.* **101,** 025503 (2008).
5. Warner, D. H., Curtin, W. A. & Qu, S. Rate dependence of crack-tip processes predicts twinning trends in f.c.c. metals. *Nature Mater.* **6,** 876–881 (2007).
6. Niewczas, M. in *Dislocations in Solids* Vol. 13 (eds Nabarro, F. R. N. & Hirth, J. P.) 263–364 (Elsevier, 2007).
7. Song, S. G. & Gray, G. T. Structural interpretation of the nucleation and growth of deformation twins in Zr and Ti. *Acta Metall. Mater.* **43,** 2325–2350 (1995).
8. Williams, J. C., Baggerly, R. G. & Paton, N. E. Deformation behavior of HCP Ti-Al alloy single crystals. *Metall. Mater. Trans. A* **33,** 837–850 (2002).
9. Ogata, S., Li, J., Hirosaki, N., Shibutani, Y. & Yip, S. Ideal shear strain of metals and ceramics. *Phys. Rev. B* **70,** 104104 (2004).
10. Suresh, S. & Li, J. Deformation of the ultra-strong. *Nature* **456,** 716–717 (2008).
11. Lu, L., Chen, X., Huang, X. & Lu, K. Revealing the maximum strength in nanotwinned copper. *Science* **323,** 607–610 (2009).
12. Argon, A. S. & Yip, S. The strongest size. *Phil. Mag. Lett.* **86,** 713–720 (2006).
13. Schiotz, J. & Jacobsen, K. W. A maximum in the strength of nanocrystalline copper. *Science* **301,** 1357–1359 (2003).
14. Shan, Z. W. *et al.* Grain boundary-mediated plasticity in nanocrystalline nickel. *Science* **305,** 654–657 (2004).
15. Uchic, M. D., Dimiduk, D. M., Florando, J. N. & Nix, W. D. Sample dimensions influence strength and crystal plasticity. *Science* **305,** 986–989 (2004).
16. Shan, Z. W., Mishra, R. K., Asif, S. A. S., Warren, O. L. & Minor, A. M. Mechanical annealing and source-limited deformation in submicrometre-diameter Ni crystals. *Nature Mater.* **7,** 115–119 (2008).
17. Greer, J. R., Oliver, W. C. & Nix, W. D. Size dependence of mechanical properties of gold at the micron scale in the absence of strain gradients. *Acta Mater.* **53,** 1821–1830 (2005).
18. Meyers, M. A., Vohringer, O. & Lubarda, V. A. The onset of twinning in metals: a constitutive description. *Acta Mater.* **49,** 4025–4039 (2001).
19. Stanford, N., Carlson, U. & Barnett, M. R. Deformation twinning and the Hall-Petch relation in commercial purity Ti. *Metall. Mater. Trans. A* **39,** 934–944 (2008).
20. El-Danaf, E., Kalidindi, S. R. & Doherty, R. D. Influence of grain size and stacking-fault energy on deformation twinning in fcc metals. *Metall. Mater. Trans. A* **30,** 1223–1233 (1999).
21. Paton, N. E. & Backofen, W. A. Plastic deformation of titanium at elevated temperatures. *Metall. Trans.* **1,** 2839–2847 (1970).
22. Akhtar, A. Basal slip and twinning in alpha-titanium single-crystals. *Metall. Trans. A* **6,** 1105–1113 (1975).
23. Yoo, M. H. Twinning and mechanical behavior of titanium aluminides and other intermetallics. *Intermetallics* **6,** 597–602 (1998).
24. Xiao, L. Twinning behavior in the Ti-5 at.% Al single crystals during cyclic loading along. *Mater. Sci. Eng. A* **394,** 168–175 (2005).
25. Svelto, O. *Principles of Lasers* (Springer, 1998).
26. Cottrell, A. H. & Bilby, B. A. A mechanism for the growth of deformation twins in crystals. *Phil. Mag.* **42,** 573–581 (1951).
27. Niewczas, M. & Saada, G. Twinning nucleation in Cu-8 at.% Al single crystals. *Phil. Mag. A* **82,** 167–191 (2002).
28. Song, S. G. & Gray, G. T. Double dislocation pole model for deformation twinning in fcc lattices. *Phil. Mag. A* **71,** 661–670 (1995).
29. El-Azab, A. The statistical mechanics of strain-hardened metals. *Science* **320,** 1729–1730 (2008).
30. Zhu, T., Li, J., Samanta, A., Leach, A. & Gall, K. Temperature and strain-rate dependence of surface dislocation nucleation. *Phys. Rev. Lett.* **100,** 025502 (2008).

**Supplementary Information** is linked to the online version of the paper at www.nature.com/nature.

**Acknowledgements** We thank Q. Liu for help with EBSD experiments. This work was supported by grants from the NSFC (50671077, 50720145101, 50831004 and 50925104), the 973 Program of China (2004CB619303, 2007CB613804 and 2010CB613003) and the 111 Project of China (B06025). J.L. was supported by ONR grant N00014-05-1-0504, NSF grant CMMI-0728069, MRSEC grant DMR-0520020 and AFOSR grant FA9550-08-1-0325. X.H. was supported by the Danish National Research Foundation. The *in situ* TEM work was performed at the National Center for Electron Microscopy, Lawrence Berkeley Laboratory, which is supported by the US Department of Energy under contract DE-AC02-05CH11231.

**Author Contributions** Q.Y. and Z.-W.S. carried out the experiments, J.L. constructed the model, X.H. interpreted the EBSD results, L.X. supervised the sample selection, J.S. designed the project, J.L. and E.M. wrote the paper. All authors contributed to the discussions.

**Author Information** Reprints and permissions information is available at www.nature.com/reprints. The authors declare no competing financial interests. Correspondence and requests for materials should be addressed to J.S. (junsun@mail.xjtu.edu.cn) or J.L. (liju@seas.upenn.edu).